

1 *Revision 1*

2 *Regular article*

3 Word count: 5530

4 **Scandio-winchite, ideally $\square(\text{NaCa})(\text{Mg}_4\text{Sc})(\text{Si}_8\text{O}_{22})(\text{OH})_2$, the first Sc-dominant amphibole-**
5 **supergroup mineral from Jordanów Śląski, Lower Silesia, southwestern Poland:**
6 **description and crystal structure**

7

8 Adam Pieczka^{1*}, Marcin Stachowicz², Sylwia Zelek-Pogudz¹, Bożena Gołębiowska¹, Mateusz
9 Sęk¹, Krzysztof Nejbert², Jakub Kotowski², Beata Marciniak-Maliszewska², Adam
10 Szuszkiewicz³, Eligiusz Szełęg⁴, Katarzyna M. Stadnicka⁵, Krzysztof Woźniak⁶

11

12 ¹ *Department of Mineralogy, Petrography and Geochemistry, AGH University of Science and*
13 *Technology, Mickiewicza 30, 30-059 Kraków, Poland*

14 ² *Faculty of Geology, University of Warsaw, Żwirki and Wigury 93, 02-089 Warszawa, Poland*

15 ³ *Institute of Geological Sciences, University of Wrocław, M. Borna 9, 50-204 Wrocław, Poland*

16 ⁴ *University of Silesia, Faculty of Natural Sciences, Institute of Earth Sciences, Będzińska 60, 41-*
17 *200 Sosnowiec, Poland*

18 ⁵ *Faculty of Chemistry, Jagiellonian University in Kraków, Gronostajowa 2, 30-387 Kraków,*
19 *Poland*

20 ⁶ *Department of Chemistry, University of Warsaw, Pasteura 1, 02-093 Warszawa, Poland*

21 *e-mail: pieczka@agh.edu.pl

22

Abstract

23 Scandio-winchite, the first natural Sc-dominant amphibole-supergroup mineral, has been
24 discovered in a granitic pegmatite that crops out in close association with rodingite-like calc-
25 silicate rocks and metasomatized granitic bodies in a serpentinite quarry at a Jordanów Śląski
26 village near Sobótka, ~30 km south of Wrocław, Lower Silesia, SW Poland. It occurs as an
27 isolated subhedral crystal, with the size of $\sim 20 \times 8 \mu\text{m}$ in planar section, and as three
28 polycrystalline aggregates, up to $50 \mu\text{m}$ across, composed of needle-shaped crystals dominated
29 by $\{110\}$. It is present within chlorite aggregates that supposedly represent remnants of partly
30 recrystallized xenoliths of the blackwall chlorite schists and in quartz-feldspar portions of the
31 pegmatite adjoining such xenolithic assemblages. Owing to the scarcity of the material and
32 exceptionally small size of the crystals, color, streak, and optical properties could not be
33 measured. By analogy with other amphiboles, scandio-winchite has a vitreous luster, brittle
34 tenacity, and a Mohs hardness of $\sim 5\frac{1}{2}$. The mineral shows an uneven fracture and $\{110\}$ perfect
35 cleavage, with an angle of $\sim 56^\circ$ between cleavage planes. The density calculated from the
36 empirical formula and refined unit-cell parameters is $3.026 \text{ g}\cdot\text{cm}^{-3}$. The holotype crystal is
37 composed of (in wt%): 55.88 SiO₂, 0.11 TiO₂, 0.53 Al₂O₃, 9.22 Sc₂O₃, 0.44 MnO, 8.89 FeO,
38 12.77 MgO, 5.71 CaO, 4.12 Na₂O, 0.17 K₂O, and 2.09 H₂O⁽⁺⁾_{calc.}; total 99.93. The composition
39 normalized on the basis of 22 O²⁻ + 2 (OH)⁻ ions corresponds to the empirical formula
40 $^A(\square_{0.966}\text{K}_{0.031}\text{Na}_{0.003})_{\Sigma 1}^B(\text{Na}_{1.132}\text{Ca}_{0.868})_{\Sigma 2}^C(\text{Mg}_{2.704}\text{Fe}^{2+}_{1.055}\text{Mn}_{0.053}\text{Sc}_{1.140}\text{Al}_{0.023}\text{Ti}_{0.012})_{\Sigma 4.987}^T(\text{Si}_{7.935}\text{Al}_{0.065})_{\Sigma 8.000}\text{O}_{22}(\text{OH})_2$, simplified formula $(\square, \text{K})(\text{Na}, \text{Ca})_2[(\text{Mg}, \text{Fe})_4\text{Sc}](\text{Si}_8\text{O}_{22})(\text{OH})_2$, and the ideal
41 formula $\square(\text{NaCa})(\text{Mg}_4\text{Sc})(\text{Si}_8\text{O}_{22})(\text{OH})_2$. The crystal-structure was refined in the monoclinic
42 system, space-group symmetry $C2/m$, with R_1 index of 6.57%. Its unit-cell parameters are: $a =$
43 $9.864(2) \text{ \AA}$, $b = 18.163(3) \text{ \AA}$, $c = 5.3053(16) \text{ \AA}$, $\beta = 104.41(3)^\circ$, $V = 920.6(4) \text{ \AA}^3$; $Z = 2$, and the
44 $a:b:c$ ratio is 0.5431 : 1 : 0.2921. The crystal-structure refinement indicates almost exclusively
45

46 Si-occupied T sites, the M4 sites occupied by nearly equal amounts of Na and Ca, M1 and M3
47 sites by divalent Mg + Fe cations, and M2 filled in equal proportions by divalent cations and Sc.
48 These results, along with the dominant vacancy at the A site, univocally indicate that the mineral
49 corresponds to a M^2Sc -analog of winchite. Scandio-winchite is most likely a secondary phase of
50 metasomatic origin related to the evolution of the country rocks and partial alteration of the
51 blackwall chlorite schists xenolith induced by the pegmatitic melt and associated fluids.

52

53 Keywords: scandium, new species of amphibole, scandio-winchite, composition, structure
54 refinement, Jordanów Śląski, Poland.

55

56

Introduction

57 Although scandium (Sc) has long been known as a trace constituent in amphiboles, reports
58 documenting Sc as a major constituent are extremely rare. Foord et al. (1993) documented up to
59 1.7 wt% Sc_2O_3 in edenite and up to 2.9 wt% Sc_2O_3 in actinolite from granitic pegmatites and the
60 metagabbro host from the Crystal Mountain fluorite deposit, Ravalli County, Montana, U.S.A.
61 Pieczka et al. (in press) reported actinolite evolving to scandio-winchite with up to 5.45 wt%
62 Sc_2O_3 from a granitic pegmatite in a serpentinite quarry at Jordanów Śląski in Lower Silesia,
63 Poland. We here provide a formal description of scandio-winchite from Jordanów Śląski.

64 Scandium is considered a C-group cation in amphiboles, with the general formula

65 $AB_2C_5T_8O_{22}W_2$ (Hawthorne et al. 2012, modified), where:

66 A = □, Na, K, Ca, Pb, and Li;

67 B = Na, Ca, Mn^{2+} , Fe^{2+} , Mg, and Li;

68 C = Mg, Fe^{2+} , Mn^{2+} , Zn, Co, Ni, Al, Fe^{3+} , Mn^{3+} , Sc^{3+} , Cr^{3+} , V^{3+} , Ti^{4+} , Zr, and Li;

69 T = Si, Al, Ti^{4+} , and Be;

70 $W = (\text{OH}), \text{F}, \text{Cl}, \text{ and } \text{O}^{2-}$.

71 Studies of synthetic scandian analogs of fluor-eckermannite, fluor-nybøite, pargasite, and fluor-
72 pargasite show that Sc is ordered mainly at the M2 sites (Raudsepp et al. 1987a, b, 1991; Oberti
73 et al. 1999).

74 Scandio-winchite is the first naturally occurring amphibole with Sc-dominant M2 sites. Its
75 name (symbol Swnc) conforms to the nomenclature of the amphibole supergroup (Hawthorne et
76 al. 2012), by analogy with winchite, $\square(\text{NaCa})(\text{Mg}_4\text{Al})(\text{Si}_8\text{O}_{22})(\text{OH})_2$, and ferri-winchite,
77 $\square(\text{NaCa})(\text{Mg}_4\text{Fe}^{3+})(\text{Si}_8\text{O}_{22})(\text{OH})_2$, of the sodium-calcium amphiboles subgroup [as defined by
78 $0.75 > {}^B(\text{Ca} + \Sigma\text{M}^{2+})/\Sigma\text{B} > 0.25$, ${}^B\text{Ca}/\Sigma\text{B} \geq {}^B\Sigma\text{M}^{2+}/\Sigma\text{B}$ and $0.75 > {}^B(\text{Na} + \text{Li})/\Sigma\text{B} > 0.25$, ${}^B\text{Na}/\Sigma\text{B} \geq$
79 ${}^B\text{Li}/\Sigma\text{B}$]. The prefix ‘scandio’ refers to trivalent C cation (Sc) replacing Al at the M2 site in
80 winchite or Fe^{3+} in ferri-winchite. In the classification of Strunz and Nickel (2001), scandio-
81 winchite belongs to class 9DE.20 in the subgroup 9.DE: Inosilicates with 2-periodic double
82 chains, Si_4O_{11} ; Clinoamphiboles. In the classification of Dana (Gaines et al. 1997), it belongs to
83 class 66.01.03b: Inosilicates double-width, unbranched chains, ($W = 2$): Group 3, the sodic-calcic
84 amphiboles. The mineral and its name have been approved by the Commission on New Minerals,
85 Nomenclature and Classification (CNMNC) of the International Mineralogical Association under
86 the number 2022-009 (Pieczka et al. 2022). Holotype scandio-winchite (specimen J2) is
87 deposited in the collection of the Mineralogical Museum of the University of Wrocław, Poland,
88 under the catalog number MMUWr IV8118. The postal address of the museum is as follows:
89 University of Wrocław, Faculty of Earth Science and Environmental Management, Institute of
90 Geological Sciences, Mineralogical Museum, Cybulskiego 30, 50-205 Wrocław, Poland.

91

92

Occurrence

93 The type locality of scandio-winchite is a serpentinite quarry situated ~1 km west of the
94 Jordanów Śląski village near Sobótka, ~30 km south of Wrocław, Lower Silesia, SW Poland
95 (50°52'16"N; 16°50'18"E). The quarry is located near the eastern margin of a ~23 × 11 km
96 exposure of the Gogołów-Jordanów Serpentinite Massif, a part of the Ślęza Ophiolite, in the
97 Sudetes, at the northeastern margin of the Bohemian Massif in the Central European Variscides.
98 Together with gabbros, metagabbros and amphibolites cropping out to the northwest, the rocks
99 form the ~403 Ma Ślęza Ophiolite (Kryza and Pin 2010; Awdankiewicz et al. 2021). Low-
100 temperature serpentinization of the ultramafic members of the ophiolite (ocean-floor
101 metamorphism) dated at ~400 Ma was followed by low-grade regional metamorphism in the
102 suprasubduction environment (Dubińska et al. 2004; Kryza and Pin 2010).

103 The pegmatite hosting scandio-winchite intruded into a ~5 m wide NE-SW-trending steeply
104 zone, traditionally called 'a leucocratic zone', that cuts the serpentinites in the western part of the
105 quarry. This zone is built mainly of rodingite-like calc-silicate rocks and partly metasomatized
106 granite bodies. The rodingitic rocks formed at the expense of a plagiogranitic precursor and
107 mainly consist of grossular-rich garnet, zoisite, clinozoisite, epidote, and diopside, among others
108 (e.g., Heflik 1967, 1982; Majerowicz 1984; Dubińska and Szafranek 1990; Dubińska 1995,
109 1997). The granite contains quartz, albite and K-feldspar with locally abundant grossular-rich
110 garnet and actinolite with accessory apatite and zircon, and was dated at ~340 Ma (Kryza 2011).
111 The granite locally lacks garnet and contains abundant zoisite and minor diopside. The
112 exocontact of the leucocratic zone with the surrounding serpentinite consists of discontinuous and
113 tectonically disrupted blackwall schists, from a few cm to ~1 m thick, containing mostly chlorite,
114 vermiculite, tremolite, and locally also talc (Dubińska and Wiewióra 1988; Dubińska and
115 Szafranek 1990). The blackwall encloses also irregular bodies of rocks transitional between
116 nephrite and serpentinite containing antigorite, tremolite and chlorite with minor actinolite and

117 diopside (Gil 2013; Gil et al. 2015, 2020). The serpentinite consists of antigorite with minor
118 chrysotile. The rocks of the leucocratic zone and the blackwall were sheared and brecciated to a
119 variable extent and interlock with each other, with intricate and often ambiguous structural
120 relationships. They are also overprinted by late-stage hydrothermal and supergene alterations. At
121 the present state of the exposure, the pegmatite with scandio-winchite cannot be observed in the
122 quarry walls, and its relation to other lithologies of the leucocratic zone is ambiguous. Earlier
123 field observations allude to irregular pegmatitic segregations and veins, typically from several
124 centimeters to slightly over 10 cm thick, within fine-grained aplite (Waleńczak 1969; Lis and
125 Sylwestrzak 1981). The age of the pegmatite remains unconstrained.

126 Scandio-winchite was found in a sample of the pegmatite collected in the 1990s by A.P. The
127 rock is coarse-grained, undeformed, composed mainly of quartz, sodic plagioclase and K-feldspar
128 with accessory pale green to nearly colorless beryl and dark green dravitic tourmaline. It also
129 contains scattered aggregates of greenish yellow clinocllore that we interpret as mechanically
130 introduced small fragments of partly recrystallized blackwall schist (detailed description in
131 Pieczka et al. in press). Systematic investigations using electron microprobe, supported in some
132 cases by Raman spectroscopy, revealed the presence of actinolite, aikinite, allanite-(Ce),
133 bavenite-bohseite, biotite, cassiterite, clinozoisite, columbite-(Mn), diopside, epidote, euxenite-
134 (Y), fersmite, fluorapatite, galena, milarite, monazite-(Ce), muscovite, phenakite, pyrochlore- and
135 microlite-group minerals, rhabdophane-(La), rhabdophane-(Ce), rhabdophane-(Nd), spessartine,
136 titanite, tremolite, zircon, uraninite, and xenotime-(Y). Pieczka et al. (in press) described
137 cascandite and Sc-rich actinolite evolving to scandio-winchite, and contended that the Sc-rich
138 amphiboles are most likely of metasomatic origin related to the metamorphic evolution of the
139 country rocks and partial alteration of the blackwall chlorite schists xenolith.

140

141

Appearance and physical properties

142 In the granitic pegmatite, scandio-winchite occurs within chlorite-dominated mineral aggregates
143 that supposedly represent remnants of partly recrystallized xenoliths of the blackwall chlorite
144 schists and in quartz-feldspar portions of the pegmatite adjoining such xenolithic assemblages. It
145 was found as an isolated subhedral crystal, with the size of $\sim 20 \times 8 \mu\text{m}$ in planar section (Fig. 1),
146 and as three polycrystalline aggregates, up to $\sim 50 \mu\text{m}$ across, composed of subhedral to euhedral
147 needle-shaped untwinned crystals with the $\{110\}$ form prominent (Fig. 2). Color, streak, and
148 optical properties could not be observed owing to exceptionally small crystal sizes. By analogy
149 with other amphibole-group minerals, scandio-winchite very likely has a vitreous luster, brittle
150 tenacity, and a Mohs hardness $\sim 5\frac{1}{2}$. The mineral shows an uneven fracture and $\{110\}$ perfect
151 cleavage, with an angle of $\sim 56^\circ$ between cleavage planes measured in the section roughly
152 perpendicular to the elongation (Figs 1, 2). Density could not be measured directly because of
153 extremely small volume of the mineral. The density calculated from the empirical formula and
154 unit-cell parameters is $3.026 \text{ g}\cdot\text{cm}^{-3}$. Scandio-winchite is biaxial, with a mean refractive index
155 close to 1.641, the value obtained from the Gladstone-Dale relation (Mandarino 1979, 1981)
156 using the empirical formula and calculated density.

157

158

Chemical composition

159 A quantitative chemical analysis of scandio-winchite was performed with a CAMECA SX 100
160 electron probe micro-analyzer (EPMA) operating in wavelength-dispersive X-ray spectrometry
161 mode (WDS), at the Inter-Institute Analytical Complex for Minerals and Synthetic Substances at
162 the University of Warsaw, Poland. Owing to small sizes of the J2d crystal (sample J2), the
163 analysis was made only in three spots located in its center (Fig. 1). The following operating
164 conditions were used: accelerating voltage 15 kV; beam current 20 nA; beam diameter $2 \mu\text{m}$;

165 peak and background count times 20 and 10 s, respectively. The analytical reference materials,
166 emission lines, diffracting crystals, and mean detection limits in wt.% element were: diopside:
167 Mg ($K\alpha$, TAP, 0.02), Si ($K\alpha$, TAP, 0.03), and Ca ($K\alpha$, LPET, 0.02), albite: Na ($K\alpha$, TAP, 0.06),
168 orthoclase: Al ($K\alpha$, LPET, 0.02) and K ($K\alpha$, LPET, 0.02), metallic Sc: Sc ($K\alpha$, LPET, 0.02),
169 rutile: Ti ($K\alpha$, LPET, 0.02), rhodonite: Mn ($K\alpha$, LIF, 0.06), and hematite: Fe ($K\alpha$, LIF, 0.06).
170 Fluorine ($K\alpha$, PC0, 0.13) and Zr ($K\alpha$, LIF, 0.05) were sought for but found below detection
171 limits. The raw data were reduced with the PAP routine (Pouchou and Pichoir 1991). Water
172 content was not measured directly owing to the scarcity of the type material. Atomic contents in
173 the empirical amphibole formula were normalized on the basis of $22 \text{O}^{2-} + 2 (\text{O}, \text{OH})^{-}$ anions per
174 formula unit (pfu) using the Excel spreadsheet designed to classify amphiboles (Locock 2014)
175 according to the IMA 2012 recommendations (Hawthorne et al. 2012). The amount of OH was
176 estimated from the equation $\text{OH} = 2 - 2^{\text{C}}\text{Ti}$ pfu. The EPMA results for the crystal J2d used for
177 structure refinement are presented in Table 1a.

178 The empirical formula of the J2d crystal is

179 $^{\text{A}}(\square_{0.965}\text{K}_{0.031}\text{Na}_{0.004})_{\Sigma 1}^{\text{B}}(\text{Na}_{1.131}\text{Ca}_{0.869})_{\Sigma 2}^{\text{C}}(\text{Mg}_{2.705}\text{Fe}^{2+}_{1.056}\text{Mn}_{0.053}\text{Sc}_{1.141}\text{Al}_{0.027}\text{Ti}_{0.012})_{\Sigma 4.994}^{\text{T}}(\text{Si}_{7.939}\text{A}$
180 $\text{l}_{0.061})_{\Sigma 8.000}\text{O}_{22}(\text{OH}_{1.975}\text{O}_{0.025})_2$. It leads to the simplified formula

181 $(\square, \text{K})(\text{Na}, \text{Ca})_2[(\text{Mg}, \text{Fe})_4\text{Sc}](\text{Si}_8\text{O}_{22})(\text{OH})_2$ and the ideal formula $\square(\text{NaCa})(\text{Mg}_4\text{Sc})(\text{Si}_8\text{O}_{22})(\text{OH})_2$,

182 which requires (in wt%) 58.91 SiO₂, 19.76 MgO, 8.45 Sc₂O₃, 6.87 CaO, 3.80 Na₂O, and 2.21

183 H₂O; Total 100. Compositions of the crystals J2a-c from the same sample (Fig. 2) correspond to

184 the same simplified and idealized formula and their empirical formulae are shown in Table 1b.

185 Chemical compositions of all the crystals studied are plotted in the classification diagram for the

186 Na–Ca amphibole subgroup (Fig. 3).

187

188

Crystallography

189 **Powder X-ray diffraction**

190 Powder X-ray diffraction data could not be collected owing to the scarcity and heterogeneity of
191 the scandio-winchite crystals. Therefore, the powder pattern was calculated from the crystal
192 structure of the crystal J2d using the Diamond program, Version 3.2k (Crystal Impact 2014). The
193 seven strongest reflections are [d in Å (*I*) *hkl*]: 8.45 (100) 110; 3.405 (45.15) 131; 3.137 (61.64)
194 310; 2.724 (85.61) 151; 2.608 (26.76) 061; 2.542 (47.76) -202; 2.345 (26.99) -351. The complete
195 calculated powder X-ray diffraction data are available as a supplementary material (SM1).

196

197 **Single-crystal X-ray diffraction and structure refinement**

198 A single crystal of scandio-winchite J2d ($24 \times 20 \times 4 \mu\text{m}$) was extracted in the Laboratory of
199 Transmission Electron Microscopy, Academic Centre for Materials and Nanotechnology
200 (ACMiN, AGH University of Science and Technology, Kraków, Poland), using Quanta 3D 200i
201 (Thermo Fisher Scientific) scanning electron microscope equipped with Ga⁺ ion gun, Pt
202 precursor gas injection systems (GIS) and Omniprobe micromanipulator for *in situ* lift-out. An
203 ion beam accelerating voltage of 30 kV and ion currents in the range of 60 nA to 1 nA were
204 applied. The sample was transferred *via* a micromanipulator to standard TEM copper half-ring
205 grids. The FIB deposition process (from Pt precursor) was used to attach the manipulator probe to
206 the sample and the foil to the grid. Subsequently, the copper grid was manually removed and the
207 crystal was transferred to a suitable microloop and placed on the goniometer base.

208 Single-crystal X-ray studies were carried out with four-circle diffractometer SuperNova,
209 equipped with an Atlas (Rigaku Oxford Diffraction) charge-coupled device detector. The
210 detector-to-crystal distance was 55.0 mm. We employed CuK α radiation ($\lambda = 1.54184\text{\AA}$) at 50.00
211 kV and 0.80 mA. The crystal was attached to a non-diffracting Mitegen micromount support. A

212 frame-width of 1° in ω scans and a frame-time of 150 and 300s were used in the data collection
213 strategy. Reflection intensities were corrected for Lorentz, polarization and absorption effects and
214 converted to structure factors using the CrysAlisPro 1.171.41.93a (Rigaku Oxford Diffraction
215 2020) software.

216 The crystal structure of scandio-winchite was solved with dual-space iterative phasing
217 algorithm implemented in ShelXT (Sheldrick 2015a) that located positions of all cations (except
218 hydrogen) and O anions. Correct element-assignment for cations and anions was based upon
219 compositional data obtained by EPMA and crystal-chemical reasoning, comprising site-
220 scattering, coordination and bond lengths. The model was refined with the least-squares
221 minimization to $R_1 = 6.57\%$ using Shelxl (Sheldrick 2015b), within the Olex2 (Dolomanov et al.
222 2009) graphical interface. Where more than one element occupies the same position in the
223 asymmetric unit, constraints for equal atom coordinates and equal anisotropic displacement
224 parameters for these groups of atoms within each unique site were applied.

225 The occupancies of T2, M1, M2, M3, and M4 sites were refined as Si vs. Al, Mg vs. Fe, Mg
226 vs. Sc, Mg vs. Fe, and Ca vs. Na, respectively, assuming full occupancy of the sites. The T1 site-
227 occupancy was fixed as $\text{Si}_{1.00}$, and 0.03 apfu K was fixed at the A site. Data collection and
228 structure refinement details as well as the refined-formula are presented in Table 2. Atom
229 positions, equivalent isotropic and anisotropic displacement parameters, and selected interatomic
230 distances are in the attached CIF file accessible as a supplementary material SM2; Table 3
231 presents assigned site-populations, and Table 4 provides bond-valence analysis of scandio-
232 winchite.

233

234 **Crystal structure**

235 Scandio-winchite crystallizes in space group $C2/m$ (#12). Its structure is typical for monoclinic
236 amphiboles, with unit-cell parameters: $a = 9.864(2) \text{ \AA}$, $b = 18.163(3) \text{ \AA}$, $c = 5.3053(16) \text{ \AA}$, $\beta =$
237 $104.41(3)^\circ$, $V = 920.6(4) \text{ \AA}^3$; $Z = 2$. The $a:b:c$ ratio calculated from the unit-cell parameters is
238 $0.5431 : 1 : 0.2921$.

239 An initial refinement of the structure indicated that the tetrahedral T1 and T2 sites are
240 occupied almost exclusively by Si. Therefore, in the final refinement, occupancies of the sites
241 were fixed to ${}^{\text{T1}}\text{Si}_{1.00}$ and ${}^{\text{T2}}(\text{Si}_{0.985}\text{Al}_{0.015})$, corresponding to electron densities at the sites
242 expected from the empirical formula of the refined crystal J2d. In other crystals of scandio-
243 winchite from the same sample, mean site-scattering powers derived from empirical formulae
244 (Table 1b) are comparable with the crystal J2d (J2a: 14.02 e^- ; J2b: 14.00 e^- ; J2c: 13.98 e^-).
245 Altogether, they indicate that the tetrahedral sites in scandio-winchite are occupied exclusively,
246 or almost exclusively, by Si. Both tetrahedra types are variably distorted, with bond lengths
247 varying in the range of $1.621(6)$ – $1.635(6) \text{ \AA}$ (T1), and $1.599(5)$ – $1.669(6) \text{ \AA}$ (T2), with mean
248 values of 1.626 and 1.636 \AA , respectively. The more distorted tetrahedron T2, with slightly
249 longer $\langle\text{T2-O}\rangle$ distance, may indicate the replacement of small Si amounts by Al, Fe^{3+} , or Ti.

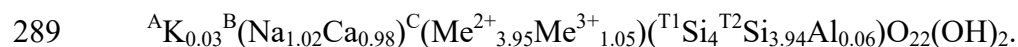
250 The occupancy of the M4 site was refined at $\text{Na}_{0.51(2)}\text{Ca}_{0.49(2)}$ with site-scattering of $15.41(18)$
251 e^- (SM2). It generally corresponds to the M4 site-occupancy calculated on the basis of B-cations
252 contents in the empirical formula of the refined J2d crystal (14.91 e^-) (Table 3). In the other
253 crystals, increased empirical mean M4 site-scattering power (J2a: 17.02 e^- ; J2b: 16.53 e^- ; J2c:
254 17.52 e^-) reflects variation in the ${}^{\text{B}}\text{Na}/{}^{\text{B}}(\text{Na}+\text{Ca})$ ratio mainly due to the coupled substitution ${}^{\text{B}}\text{Na}$
255 $+ {}^{\text{C}}\text{Sc} \leftrightarrow {}^{\text{B}}\text{Ca} + {}^{\text{C}}\text{Me}^{2+}$ at the M4 and M1-M3 sites (Table 1b). The M4 site is highly distorted
256 with B–O bond-lengths ranging from $2.354(6)$ to $2.839(6) \text{ \AA}$, and mean $\langle{}^{\text{B}}(\text{Na,Ca})\text{-O}\rangle$ distance
257 2.539 \AA . The bond-valence sum (BVS) of 1.508 valence unit (vu) calculated for the site (Table 3)

258 corresponds perfectly to the ideal M4 site-population (NaCa)_{Σ2} in amphiboles of the sodium-
259 calcium subgroup of the (OH,F,Cl)-dominant amphibole group.

260 Occupancies of the five octahedral M sites (2 × M1, 2 × M2, and M3) were refined in the
261 systems Mg–Fe (M1, M3) and Mg–Sc (M2), respectively, as Mg_{0.813(14)}Fe_{0.187(14)}, Mg_{0.79(2)}Fe_{0.21(2)},
262 and Sc_{0.58(2)}Mg_{0.42(2)} (a supplementary material SM2), which correspond to the refined site-
263 scattering power 14.62(20) e⁻, 14.94(28) e⁻, and 17.22(18) e⁻ (Table 3). Bond lengths in the M1-
264 M3 octahedra vary in ranges: 2.063(6)–2.111(6), 1.997(6)–2.177(5), and 2.055(8)–2.092(5) Å,
265 with almost identical <M–O> distances of 2.085, 2.089 and 2.080 Å. The total refined scattering
266 at the M1–M3 sites, 78.62 e⁻, differs from that of 85.71 e⁻ calculated from the empirical EPMA
267 formula for the refined crystal J2d. We suspect that the main reason for the difference lies in the
268 non-ideal quality of the extracted crystal. Crystal J2d is exceptionally small and shows a
269 heterogeneous distribution of Mg and Sc, the constituents of the sites M1–M3, and Ca and Na,
270 the constituents of the M4 site (Fig. 1c-g). The EPMA spot analyses were made in the central part
271 of the crystal, particularly rich in Sc and poor in Mg, to restrict contamination by the surrounding
272 clinocllore mass. However, outer parts of the crystal are richer in Mg and Ca, and poorer Sc and
273 Na, which suggest the replacement ^BCa + ^CMg → ^BNa + ^CSc. Thus, the three EPMA analyses
274 can be slightly non-representative in respect to the whole volume of the extracted crystal. The
275 same applies to other investigated crystals of scandio-winchite. Consequently, the M site-
276 occupancies in the refined formula presented in Table 2 deviate slightly from the real ones.

277 However, more accurate assignments of the M1–M3 site-populations in the refined crystal J2d
278 can be calculated in the following manner. Assuming that the homovalent substitution ^MSc →
279 ^MAl is negligible, approximate quantitative relationships among ^CMe²⁺ (Mg, Fe, and Mn) and
280 ^CMe³⁺ (Sc and Al) occupants can be estimated from stoichiometry. The ideal scandio-winchite
281 composition, □(NaCa)(Mg₄Sc)(Si₈O₂₂)(OH)₂, can be derived from tremolite,

282 $\square(\text{CaCa})\text{Mg}_5(\text{Si}_8\text{O}_{22})(\text{OH})_2$, by the aforementioned complex substitution $^{\text{M4}}\text{Ca} + ^{\text{M1-M3}}\text{Mg} \rightarrow$
283 $^{\text{M4}}\text{Na} + ^{\text{M1-M3}}\text{Sc}$. The substitution defines the content of trivalent C cations at the M1-M3 sites as
284 being equal to the $^{\text{B}}\text{Na}$ content at the M4 site. Because the M4 site-occupancy was refined as
285 $\text{Na}_{0.51(2)}\text{Ca}_{0.49(2)}$ in crystal J2d, it is reasonable to expect $^{\text{M1-M3}}\text{Me}^{3+}$ in the amount of $2 \times 0.51(2) =$
286 $1.02(4)$ apfu. In view of small amounts of additional substituents, confirmed by the EPMA results
287 and fixed at the T2 site (0.06 apfu Al) and A site (0.03 apfu K), the composition of this crystal
288 should correspond to:



290 Because the EPMA-derived formula indicates trace amounts of Al at the M1-M3 sites, we
291 assigned a small amount of $^{\text{C}}\text{Al} = 0.03$ apfu during optimization of the M1, M2 and M3
292 populations according to suggestions of Hawthorne et al. (2012). Thus, the aforementioned
293 formula used in the optimization procedure takes the final form:



295 It is worth to notice that this formula is very close to the ideal stoichiometry of the winchite-
296 subgroup species, $\square(\text{NaCa})(\text{Me}^{2+}_4\text{Me}^{3+})(\text{Si}_8\text{O}_{22})(\text{OH})_2$. Besides, it indicates lower contents of Sc
297 than in the EPMA-derived formula, as expected from the observation that EPMA analyses were
298 done in the relatively Sc-rich core of the crystal, while also relatively Sc-poor marginal parts
299 were included in the structural studies. It is also noteworthy that the difference between the
300 EPMA-derived formula and the formula calculated on the basis of the amphibole stoichiometry is
301 within 3 standard deviations of the refined Na, Ca, and Sc contents

302 The contents of $^{\text{C}}\text{Mg}$ and $^{\text{C}}\text{Fe}^{2+}$ were further optimized from a system of linear equations:

303 (1) $^{\text{C}}\text{Mg} + ^{\text{C}}\text{Fe}^{2+} + ^{\text{C}}\text{Sc} + ^{\text{C}}\text{Al} = 5$ apfu and

304 (2) $12^{\text{C}}\text{Mg} + 26^{\text{C}}\text{Fe}^{2+} + 21^{\text{C}}\text{Sc} + 13^{\text{C}}\text{Al} = 78.62$ vu,

305 where Mg, Fe²⁺, Sc, Fe³⁺, and Al denote contents of the respective C-group elements at the M1-
306 M3 sites. Accepting all Sc (1.02 apfu) entirely at the M2 site as proposed by Hawthorne et al.
307 (2012), the optimized cation-populations at the M1-M3 sites are:

308 M1: Mg_{1.63}Fe²⁺_{0.37},

309 M2: Sc_{1.02}Mg_{0.89}Fe²⁺_{0.09}, and

310 M3: Mg_{0.76}Fe²⁺_{0.21}Al_{0.03},

311 with calculated site-scattering values corresponding to the refined values and mean bond-lengths
312 differing from the refined ones by 0.006–0.007 Å per a site (Table 3). Thus the optimized
313 structural formula of the scandio-winchite J2d is:

314
$$^A(\square_{0.97}\text{K}_{0.03})^{M4}(\text{Na}_{1.02}\text{Ca}_{0.98})[^{M1}(\text{Mg}_{1.63}\text{Fe}^{2+}_{0.37})^{M2}(\text{Sc}_{1.02}\text{Mg}_{0.89}\text{Fe}^{2+}_{0.09})^{M3}(\text{Mg}_{0.76}\text{Fe}^{2+}_{0.21}\text{Al}_{0.03})]$$

315
$$[(^{T1}\text{Si}_4\ ^{T2}(\text{Si}_{3.94}\text{Al}_{0.06}))]\text{O}_{22}(\text{OH})_2.$$

316 Table 4 presents a bond-valence analysis for the case. It confirms that divalent cations (Mg, Fe)
317 dominate at the M1 and M3 sites and Sc prevails at the M2 site. The distribution of C cations at
318 the M1–M3 sites, along with the dominant vacancy at the A site, the M4 site populated by Na +
319 Ca, the T sites occupied almost exclusively by Si, and the presence of OH at the W site
320 univocally indicate that the new mineral corresponds to a ^{M2}Sc-analog of winchite. In accordance
321 with the current nomenclature of the amphibole supergroup (Hawthorne et al. 2012), the new
322 species is named scandio-winchite. Table 5 gives idealized site-occupancies in currently known
323 and hypothetical mineral species of the winchite root-name of the Na-Ca amphibole subgroup.

324

325

Implications

326 Finding of scandio-winchite is significant for two reasons. Although amphiboles, along with
327 clinopyroxenes, are regarded as major carriers of Sc among common rock-forming minerals
328 (Williams-Jones and Vasyukova 2018, and references therein), examples of amphiboles with

329 Sc₂O₃ contents at the level of a few percent are extremely rare. They are so far restricted to two
330 occurrences of pegmatitic rocks emplaced into mafic-ultramafic host rocks (Foord et al. 1993;
331 Pieczka et al. in press). In both cases, Sc is believed to have been introduced to the pegmatites
332 from the wallrocks by contamination or metasomatic alteration or both. A detailed discussion of a
333 possible mode of origin of scandian actinolite evolving to scandio-winchite from Jordanów Śląski
334 is given by Pieczka et al. (in press). In general, reaction zones between felsic and mafic-
335 ultramafic rock types seem to represent environments particularly favorable for the formation of
336 Sc-rich amphiboles. Although a transfer of many elements (e.g. Ca, Mg, Fe, Ti, Si, Na, and K
337 among others) across such zones has been extensively studied, little attention has been paid to the
338 geochemical behavior of Sc. The identification of scandio-winchite proves that the role of
339 amphiboles in controlling the mobility of scandium in such environments may be more important
340 than previously thought. The second important issue arising from this work is demonstration that
341 incorporation of Sc into the amphibole structure is facilitated by increased Na activity in the
342 crystallization environment. Because Sc enters the ^CM2 site through the heterovalent substitution
343 $M^4Na^+ + M^2Sc^{3+} \leftrightarrow M^4Ca^{2+} + M^2(Mg^{2+}, Fe^{2+})$, it may achieve higher concentrations in amphiboles
344 of the calcium-sodium or even sodium subgroups compared to the calcium subgroup.
345 Amphiboles in the reaction zone between the granitic rocks and serpentinites at Jordanów Śląski
346 are represented mainly by tremolite and actinolite (e.g. Gil et al. 2015, 2020 and references
347 therein), i.e. calcium-subgroup species. Some actinolite crystals formed within the pegmatite
348 accumulated Sc as a major constituent as a result of the aforementioned substitution. Scandium-
349 dominant species could crystallize locally only where the metasomatic fluid became sufficiently
350 enriched in Na.

351

352

Acknowledgements

353 We thank Robert F. Martin, two anonymous reviewers and the Associate Editor, Fabrizio
354 Nestola, for their thorough and inspiring reviews as well as editorial handling that greatly
355 improved the quality of the manuscript. We are also very grateful to Robert F. Martin for
356 language corrections. This study was supported by the National Science Centre (Poland) grant
357 2019/33/B/ST10/00120 to AP.

358

359

References

360 Awdankiewicz, M., Kryza, R., Turniak, K., Ovtcharova, M., and Schaltegger, U. (2021) The
361 Central Sudetic Ophiolite (European Variscan Belt): Precise U–Pb zircon dating and
362 geotectonic implications. *Geological Magazine*, 158, 555–566.

363 Crystal Impact (2014) *Diamond - Crystal and Molecular Structure Visualization*, Dr. H. Putz &
364 Dr. K. Brandenburg GbR, Kreuzherrenstr. 102, 53227 Bonn, Germany,
365 <http://www.crystalimpact.com/diamond>.

366 Dolomanov, O.V., Bourhis, L.J., Gildea, R.J., Howard, J.A.K., and Puschmann, H. (2009)
367 OLEX2: a complete structure solution, refinement and analysis program. *Journal of Applied*
368 *Crystallography*, 42, 339–341.

369 Dubińska, E. (1995) Rodingites of the eastern part of the Jordanów - Gogołów serpentinite
370 massif, Lower Silesia, Poland. *The Canadian Mineralogist*, 33, 585–608.

371 Dubińska, E. (1997) Rodingites and amphibolites from the serpentinites surrounding Góry Sowie
372 block (Lower Silesia, Poland): record of supra-subduction zone magmatism and
373 serpentinitization. *Neues Jahrbuch für Mineralogie, Abhandlungen*, 171, 239–279.

374 Dubińska, E. and Szafranek, D. (1990) On the origin of layer silicates from Jordanów (Lower
375 Silesia, Poland). *Archiwum Mineralogiczne*, 46, 19–36.

- 376 Dubińska, E., and Wiewióra, A. (1988) Layer silicates in the contact zone between granite and
377 serpentinite, Jordanów, Lower Silesia, Poland. *Clay Minerals*, 23, 459–470.
- 378 Dubińska, E., Bylina, P., Kozłowski, A., Dörr, W., Nejbort, K., Schastok, J., and Kulicki, C.
379 (2004) U–Pb dating of serpentinization: hydrothermal zircon from a metasomatic rodingite
380 shell (Sudetic ophiolite, SW Poland). *Chemical Geology*, 203, 183– 203.
- 381 Foord, E.E., Birmingham, S.D., Demartin, F., Pilati, T., Gramaccioli, C.M., and Lichte, F.E.
382 (1993) Thortveitite and associated Sc-bearing minerals from Ravalli County, Montana. *The*
383 *Canadian Mineralogist*, 31, 337–346.
- 384 Gagné, O.C., and Hawthorne, F.C. (2015) Comprehensive derivation of bond-valence parameters
385 for ion pairs involving oxygen. *Acta Crystallographica*, B 71, 562–578.
- 386 Gaines, R.V., Skinner, H.C., Foord, E.E., Mason, B., and Rosenzweig, A. (1997) *Dana's New*
387 *Mineralogy*, Eighth Edition, John Wiley & Sons, Inc.
- 388 Gil, G. (2013) Petrographic and microprobe study of nephrites from Lower Silesia (SW
389 Poland). *Geological Quarterly*, 57, 395–404.
- 390 Gil, G., Barnes, J.D., Boschi, C., Gunia, P., Szakmány, G., Bendő, Z., Raczynski, P., and Péterdi,
391 B. (2015) Origin of serpentinite-related nephrite from Jordanów and adjacent areas (SW
392 Poland) and its comparison with selected nephrite occurrences. *Geological Quarterly*, 59, 457–
393 472.
- 394 Gil, G., Bagiński, B., Gunia, P., Madej, S., Sachanbiński, M., Jokubauskas, P., and Belka, Z.,
395 (2020) Comparative Fe and Sr isotope study of nephrite deposits hosted in dolomitic marbles
396 and serpentinites from the Sudetes, SW Poland: implications for Fe-As-Au-bearing skarn
397 formation and post-obduction evolution of the oceanic lithosphere. *Ore Geology Reviews*,
398 118, 103335.

- 399 Hawthorne, F.C., Oberti, R., Harlow, G.E., Maresch, W.V., Martin, R.F., Schumacher, J.C., and
400 Welch, M.D. (2012) Nomenclature of the amphibole supergroup. *American Mineralogist*, 97,
401 2031–2048.
- 402 Heflik, W. (1967) Studium mineralogiczno-petrograficzne leukokratycznej strefy przeobrażonej
403 okolic Jordanowa Śląskiego (Dolny Śląsk). *Prace Mineralogiczne PAN*, 10, 122 p.
404 Wydawnictwa Geologiczne (in Polish).
- 405 Heflik, W. (1982) Petrographic position of rodingites from Jordanów (Lower Silesia). *Przegląd*
406 *Geologiczny*, 6, 277–280 (in Polish with English abstract).
- 407 Kryza, R. (2011) Early Carboniferous (~337 Ma) granite intrusion in Devonian (~400 Ma)
408 ophiolite of the Central-European Variscides. *Geological Quarterly*, 55, 213–222.
- 409 Kryza, R. and Pin, C. (2010) The Central-Sudetic ophiolites (SW Poland): Petrogenetic issues,
410 geochronology and palaeotectonic implications. *Gondwana Research*, 17, 292–305.
- 411 Lis, J. and Sylwestrzak, H. (1981) Nowy zespół mineralny w leukokratycznej strefie Jordanowa
412 k. Sobótki jego znaczenie genetyczne. *Przegląd Geologiczny*, 29, 67–71 (in Polish with
413 English summary).
- 414 Locock, A.J. (2014) An Excel spreadsheet to classify chemical analyses of amphiboles
415 following the IMA 2012 recommendations. *Computers & Geosciences*, 62, 1–11.
- 416 Majerowicz, A. (1984) Petrography and genesis of rodingites in serpentinites of the Ślęza
417 ophiolitic group. *Geologia Sudetica*, 18, 109–132 (in Polish with English summary).
- 418 Mandarino, J.A. (1979) The Gladstone-Dale relationship. Part III. Some general applications. *The*
419 *Canadian Mineralogist*, 17, 71–76.
- 420 Mandarino, J.A. (1981) The Gladstone-Dale relationship. Part IV. The compatibility concept and
421 its application. *The Canadian Mineralogist*, 19, 441–450.

- 422 Oberti, R., Hawthorne, F.C., Cámara, F., and Raudsepp, M. (1999) Unusual M^{3+} cations in
423 synthetic amphiboles with nominal fluoro-eckermannite composition: Deviations from
424 stoichiometry and structural effects of the cummingtonite component. American Mineralogist,
425 84, 102–111.
- 426 Pieczka, A., Stachowicz, M., Zelek-Pogudz, S., Gołębiowska, B., Nejbert, K., Kotowski, J.,
427 Marciniak-Maliszewska, B., Szuszkiewicz, A., Szełęg, E., Stadnicka, K.M. and Woźniak, K.
428 (2022) Scandio-winchite, IMA 2022-009. CNMNC Newsletter 67; Mineralogical Magazine,
429 86, 4–5.
- 430 Pieczka, A., Stachowicz, M., Zelek-Pogudz, S., Gołębiowska, B., Sęk, M., Nejbert, K., Kotowski,
431 J., Marciniak-Maliszewska, B., Szuszkiewicz, A., Szełęg, E., Stadnicka, K.M., and Woźniak,
432 K. (in press) Scandian actinolite from Jordanów, Lower Silesia, Poland: compositional
433 evolution, crystal structure and genetic implications. American Mineralogist. DOI:
434 10.2138/am-2022-8786.
- 435 Pouchou, J.L., and Pichoir, F. (1991) Quantitative analysis of homogeneous or stratified
436 microvolumes applying the model “PAP”. In K.F.J. Heinrich, and D.E. Newbury, Eds.,
437 Electron Probe Quantitation. Springer, Boston, MA.
- 438 Raudsepp, M., Turnock, A., Hawthorne, F.C., Sheriff, B., and Hartman J.S. (1987a)
439 Characterization of synthetic pargasitic amphiboles $NaCa_2Mg_4M^{3+}Si_6Al_2O_{22}(OH,F)_2$; $M^{3+} =$
440 Al, Cr, Ga, Sc, In) by infrared spectroscopy, Rietveld structure refinement, and ^{27}Al , ^{29}Si , and
441 ^{19}F MAS-NMR spectroscopy. American Mineralogist, 72, 580–593.
- 442 Raudsepp, M., Turnock, A., and Hawthorne, F.C. (1987b) Characterization of cation ordering in
443 synthetic scandium-fluor-eckermannite, indium-fluor-eckermannite, and scandium-fluor-
444 nyböite by Rietveld structure refinement. American Mineralogist, 72, 959–964.

- 445 Raudsepp, M., Turnock, A., and Hawthorne, F.C. (1991) Amphiboles at low pressure: what
446 grows and what doesn't. *European Journal of Mineralogy*, 3, 983–1004.
- 447 Rigaku Oxford Diffraction (2020) CrysAlisPro Software system, version 1.171.40.67a, Rigaku
448 Corporation, Wroclaw, Poland.
- 449 Shannon, R.D. (1976) Revised effective ionic radii and systematic studies of interatomic
450 distances in halides and chalcogenides. *Acta Crystallographica*, A32, 751–767.
- 451 Sheldrick, G.M. (2015a) Crystal structure refinement with SHELXL. *Acta Crystallographica*,
452 C71, 3–8.
- 453 Sheldrick, G.M. (2015b) SHELXT – Integrated space-group and crystal-structure determination.
454 *Acta Crystallographica*, A71, 3–8.
- 455 Strunz, H., and Nickel, E.H. (2001) *Strunz Mineralogical Tables, Ninth Edition*.
456 Schweizerbart'sche Verlagsbuchhandlung, Stuttgart.
- 457 Waleńczak, Z. (1969) Geochemistry of minor elements dispersed in quartz (Ge, Al, Ga, Fe, Ti, Li
458 and Be). *Archiwum Mineralogiczne*, 28, 189–335 (in Polish with English abstract).
- 459 Warr, L.N. (2021) IMA–CNMNC approved mineral symbols. *Mineralogical Magazine*, 85, 291–
460 320.
- 461 Williams-Jones, A.E., and Vasyukova, O.V. (2018) The economic geology of scandium, the runt
462 of the rare earth element litter. *Economic Geology*, 113, 973–988.

463 **Figure captions:**

464 **Figure 1.** Back-scattered electron images (**a, b**) and distribution maps of selected elements (**c–**
465 **g**) in the holotype J2d scandio-winchite crystal. Dark-grey circles in (**b**) mark places of spot
466 analyses. Sizes of the circles correspond to the used beam diameter. Abbreviations of mineral
467 names: Clc – clinochlore, Drv – dravite, Mc – microcline, Phl – phlogopite, Qz – quartz
468 (Warr 2021), Swns – scandio-winchite.

469 **Figure 2.** Back-scattered electron images and Sc X-ray element distribution maps in the other
470 analyzed scandio-winchite crystals: (**a, b**) fan-shaped scandio-winchite aggregate J2a in a
471 pegmatitic feldspar in contact with a chlorite aggregate, (**c**) polycrystalline scandio-winchite
472 aggregates in chlorite mass, (**d, e**) enlarged scandio-winchite aggregates J2b and J2c,
473 respectively, from the image **c**, (**f, g, h**) Sc X-ray maps in J2a, J2b and J2c crystals and
474 polycrystalline aggregates from the images **b, d, and e**, respectively. Dark-grey circles on BSE
475 images of the crystals in (**b, d, e**) mark places of spot analyses. Sizes of the circles correspond
476 to the used beam diameter. Abbreviations of mineral names: Ab – albite, Clc – clinochlore,
477 Ttn – titanite (Warr 2021), Swns – scandio-winchite.

478 **Figure 3.** Chemical compositions of the scandio-winchite crystals and polycrystalline
479 aggregates from Figures 1 and 2 in the classification diagram of Ca-Na amphiboles
480 (Hawthorne et al. 2012). Colors: orange – aggregate J2a; blue – aggregate J2b; green –
481 aggregate J2c; violet – crystal J2d. Full diamonds indicate average compositions.

Table 1a. Composition of scandio-winchite (in wt%; crystal J2d, n = 3).

Constituent	Mean	Range	SD	Reference Material
SiO ₂	55.88	55.74 – 56.15	0.23	diopside
TiO ₂	0.11	0.09 – 0.13	0.02	rutile
Al ₂ O ₃	0.53	0.48 – 0.61	0.07	orthoclase
Sc ₂ O ₃	9.22	9.19 – 9.24	0.03	pure Sc
MnO	0.44	0.40 – 0.46	0.03	rhodonite
FeO	8.89	8.83 – 8.96	0.06	hematite
MgO	12.77	12.70 – 12.85	0.08	diopside
CaO	5.71	5.42 – 5.89	0.25	diopside
Na ₂ O	4.12	4.02 – 4.24	0.11	albite
K ₂ O	0.17	0.16 – 0.18	0.01	orthoclase
H ₂ O ⁽⁺⁾ _{calc.}	2.09	2.10 – 2.12		
Total	99.93	99.43 – 100.59		

Table 1b. Chemical composition of other scandiowinchite crystals (wt%).

Constituent	J2a (n =4)			J2b (n = 5)			J2c (n =3)		
	mean	range	SD	mean	range	SD	mean	range	SD
SiO ₂	55.99	55.76 – 56.29	0.22	55.75	55.29 – 56.19	0.42	55.94	55.12 – 56.87	0.88
TiO ₂	0.18	0.14 – 0.20	0.03	0.09	0.06 – 0.12	0.03	0.11	0.05 – 0.18	0.07
Al ₂ O ₃	0.83	0.78 – 0.91	0.06	0.78	0.67 – 0.96	0.11	0.97	0.89 – 1.10	0.12
Sc ₂ O ₃	5.81	5.30 – 6.31	0.43	7.39	6.17 – 8.23	0.88	5.59	5.37 – 5.83	0.23
Fe ₂ O ₃	0.49	0.00 – 0.57	0.28	0.06	0.00 – 0.66	0.29	0.01	0.00 – 0.35	0.20
FeO	6.84	6.46 – 7.62	0.47	7.80	7.01 – 8.44	0.57	7.42	6.24 – 8.18	0.99
MnO	0.37	0.32 – 0.44	0.05	0.38	0.34 – 0.40	0.02	0.30	0.22 – 0.38	0.08
MgO	16.43	15.79 – 16.94	0.53	15.16	14.04 – 16.28	0.84	16.51	15.31 – 17.25	1.05
CaO	8.77	8.52 – 9.21	0.32	7.50	6.69 – 8.49	0.83	8.35	7.91 – 8.89	0.50
Na ₂ O	2.64	2.43 – 2.99	0.24	2.96	2.55 – 3.55	0.38	2.30	2.17 – 2.42	0.13
K ₂ O	0.17	0.15 – 0.22	0.03	0.16	0.11 – 0.21	0.04	0.14	0.10 – 0.21	0.06
H ₂ O _{calc.}	2.14	2.13 – 2.16		2.13	2.10 – 2.16		2.11	2.10 – 2.15	
Total	100.64	100.03 – 101.22		100.16	99.03 – 102.03		99.75	98.87 – 100.49	

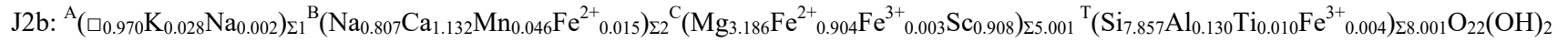


Table 2. Details on data collection and structure refinement of scandio-winchite.

Data collection and refinement:	
Instrument	SuperNova, Dual, Cu, Atlas (Rigaku - Oxford Diffraction) four circle diffractometer with a mirror monochromator
X-ray radiation source	CuK α ($\lambda = 1.54184 \text{ \AA}$)
Temperature	292(6) K
Absorption coefficient	17.58 mm ⁻¹
F(000)	832
θ range for data collection	4.870 to 72.416°
θ full	67.684°
Index ranges	-11 $\leq h \leq$ 12, -21 $\leq k \leq$ 20, -6 $\leq l \leq$ 6
Reflections collected	2833
Unique reflections	910 [$R_{\text{int}} = 0.0581$]
Reflections with $I_o > 2\sigma I$	576
Completeness to $\theta = 72.4^\circ$ (2833 reflections)	95.8%
Completeness to $\theta = 67.7^\circ$ (2753 reflections)	98.6%
Completeness to $\theta = 51.7^\circ$ (2035 reflections)	100%
Refinement method	Full-matrix least-squares on F^2
Parameters / restraints	103/1
Goodness-of-fit on F^2	1.033
Final R indices [$I_o > 2\sigma(I)$]	$R_1 = 0.0657$ $wR_2 = 0.1623$
Largest diff. peak and hole	1.017 and -0.667 e/ \AA^3 , rms = 0.194
Crystal data:	
Refined formula	^A ($\square_{0.970}\text{K}_{0.03}$) _{$\Sigma 1$} ^B (Na _{1.02} Ca _{0.98}) _{$\Sigma 2$} ^C (Mg _{3.25} Fe _{0.58} Sc _{1.17}) _{$\Sigma 5$} ^T (Si _{7.94} Al _{0.06}) _{$\Sigma 8$} O ₂₂ (OH) ₂
Crystal size	24 \times 20 \times 4 μm
Crystal system	monoclinic
Space group	$C2/m$
Unit-cell dimensions	$a = 9.864(2) \text{ \AA}$
	$b = 18.163(3) \text{ \AA}$
	$c = 5.3053(16) \text{ \AA}$
	$\alpha = 90^\circ$
	$\beta = 104.41(3)^\circ$
Unit-cell volume	$\gamma = 90^\circ$
	$V = 920.6(4) \text{ \AA}^3$
Z	2
Calculated density	3.026 g $\cdot\text{cm}^{-3}$

* $R_{\text{int}} = \Sigma |F_o^2 - F_o^2(\text{mean})| / \Sigma [F_o^2]$. GooF = $S = \{ \Sigma [w(F_o^2 - F_c^2)^2] / (n-p+r) \}^{1/2}$.
 $R_1 = \Sigma ||F_o| - |F_c|| / \Sigma |F_o|$. $wR_2 = \{ \Sigma [w(F_o^2 - F_c^2)^2] / \Sigma [w(F_o^2)^2] \}^{1/2}$; $w = 1 / [\sigma^2(F_o^2) + (aP)^2 + bP]$,
where a is 0.102, b is 0.0000 and P is $[2F_c^2 + F_o^2] / 3$.

Table 3. Assigned site-populations, total site-scattering at the sites, and mean bond-lengths for scandio-winchite.

Site	Site population	Total site-scattering (e^-)		Mean bond-length (\AA)	
		ref.	calc.	ref.	calc.
T1	Si ₄	56.00	56.00*	1.626	1.625
T2	Si _{3.94} Al _{0.06}	55.94	55.94*	1.636	1.627
M1	Mg _{1.626} Fe ²⁺ _{0.374}	29.24	29.24	2.085	2.091
M2	Sc _{1.020} Mg _{0.890} Fe ²⁺ _{0.090}	34.44	34.44	2.089	2.095
M3	Mg _{0.762} Fe ²⁺ _{0.208} Al _{0.030}	14.94	14.94	2.080	2.087
Σ(M1-M3)		78.62	78.62		
M4	Na _{1.02} Ca _{0.98}	30.82	29.81*	2.539	2.511
A	□ _{0.97} K _{0.03}	0.57	0.62*	2.960	2.95
W	(OH) ₂			0.98	

* - data derived from the EPMA formula (crystal J2d). Mean bond-lengths calculated for cation radii tabulated by Shannon (1976).

Table 4. Bond-valence ($\nu\mu$) analysis for scandio-winchite J2d.

	<i>A</i>	<i>B</i>	<i>M1</i>	<i>M2</i>	<i>M3</i>	<i>T1</i>	<i>T2</i>	H3	Σ
O1			0.351 ^{x2↓}	0.349 ^{x2↓}	0.344 ^{x4↓}	1.008			2.052
O2		0.216 ^{x2↓}	0.329 ^{x2↓}	0.420 ^{x2↓}			0.990		1.956
O3			0.367 ^{x2↓}		0.374 ^{x2↓}			0.865	1.605
O4		0.270 ^{x2↓}		0.522 ^{x2↓}			1.067		1.859
O5	0.003 ^{x4↓}	0.084 ^{x2↓}				0.972	0.941		2.000
O6	0.002 ^{x4↓}	0.183 ^{x2↓}				1.000	0.889		2.076
O7	0.009 ^{x2↓}					1.000 ^{x2→}			2.009
Σ	0.038	1.508	2.094	2.582	2.122	3.980	3.889	0.865	

Notes: Bond-valence sums were calculated using the equation $S = \exp[(R_0 - R)/B]$, where R_0 and B are bond-valence parameters derived by Gagné and Hawthorne (2015), and R is the refined bond-length.

Table 5. Scandio-winchite compared to the known and expected species of the winchite root-name of the Na-Ca amphibole subgroup in the current amphibole classification (Hawthorne et al. 2012).

	<i>A</i>	<i>B</i> ₂	<i>C</i> ₅	<i>T</i> ₈	<i>W</i> ₂
Winchite	□	NaCa	Mg ₄ Al	Si	OH
<i>Fluoro-winchite</i>	□	NaCa	Mg ₄ Al	Si	F
<i>Ferro-winchite</i>	□	NaCa	Fe ²⁺ ₄ Al	Si	OH
Ferri-winchite	□	NaCa	Mg ₄ Fe ³⁺	Si	OH
<i>Ferro-ferri-winchite</i>	□	NaCa	Fe ²⁺ ₂ Fe ³⁺ ₂	Si	OH
Scandio-winchite	□	NaCa	Mg ₄ Sc	Si	OH

Names of hypothetical species are italicized.

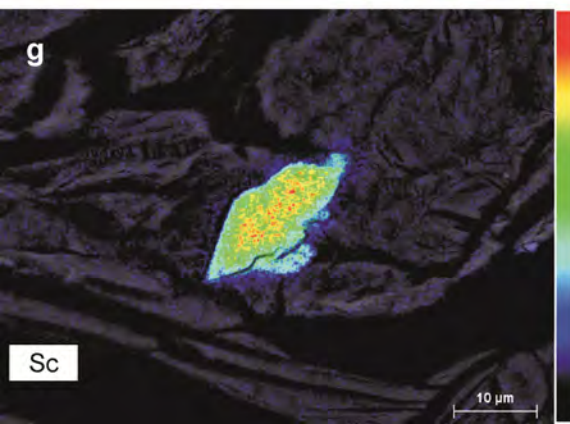
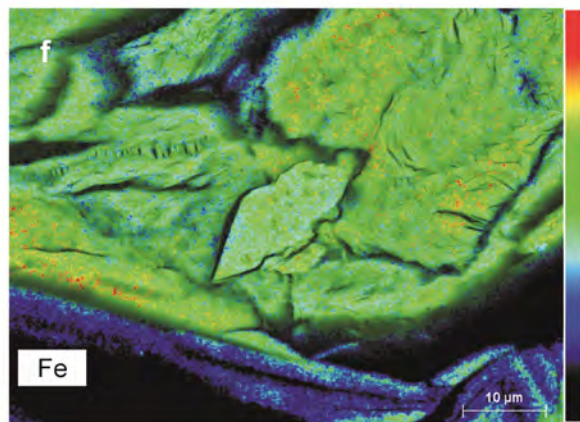
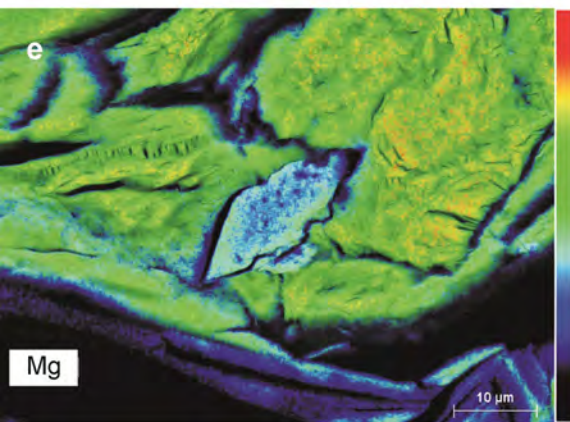
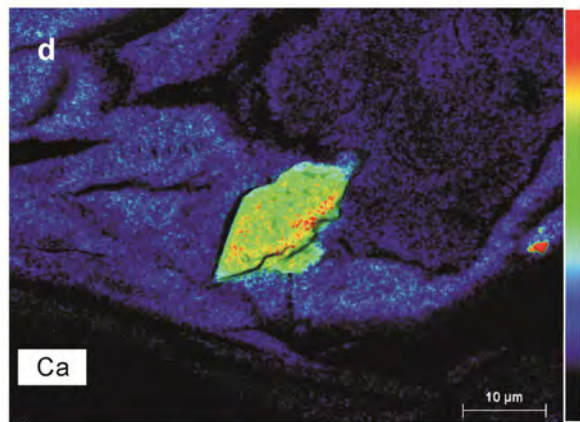
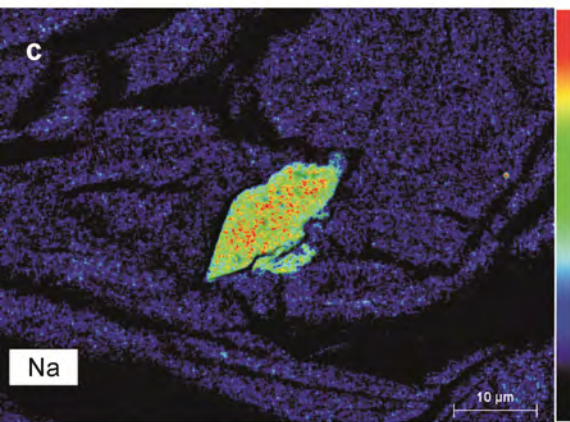
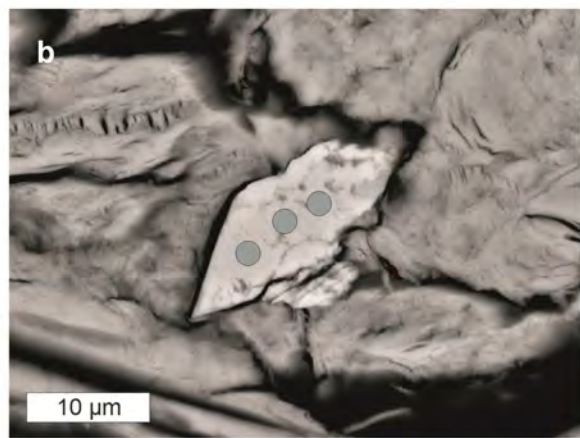
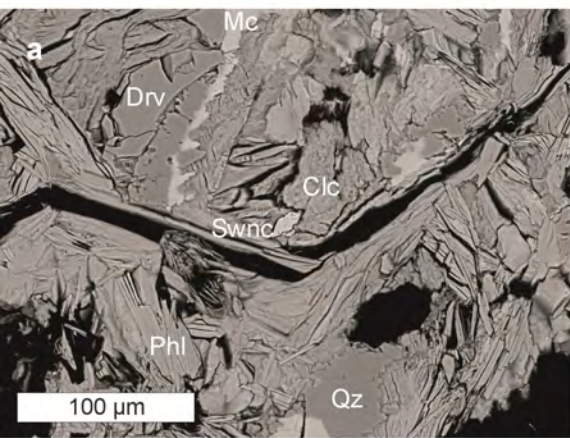


Fig. 2_Pieczka et al._Scandio-winchite

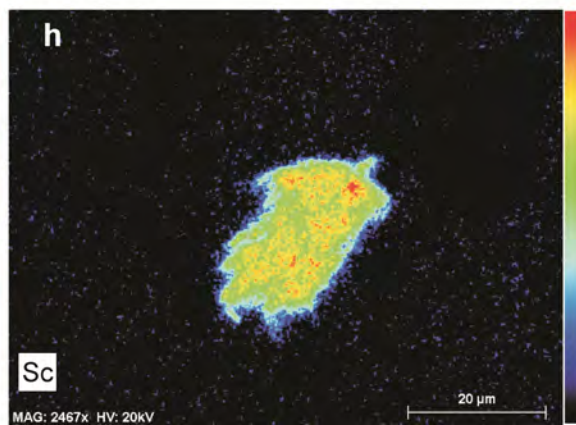
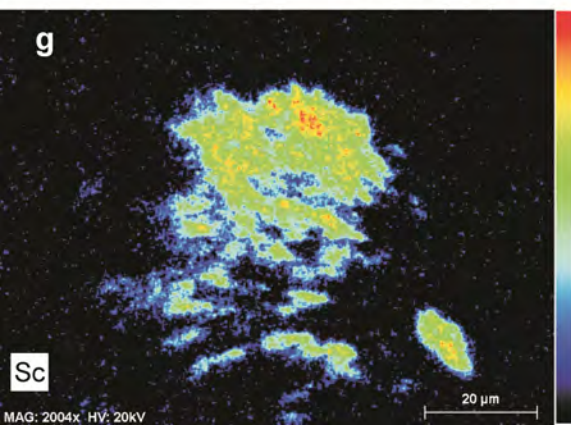
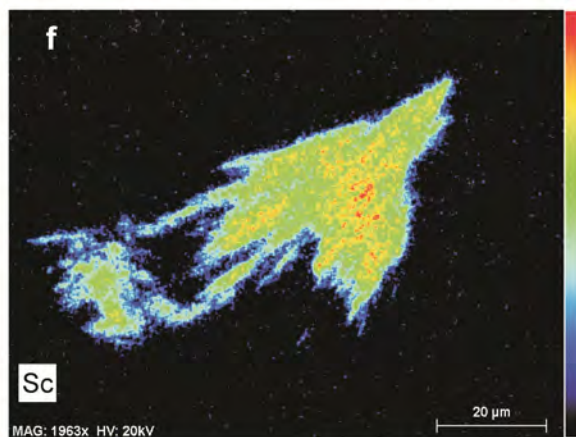
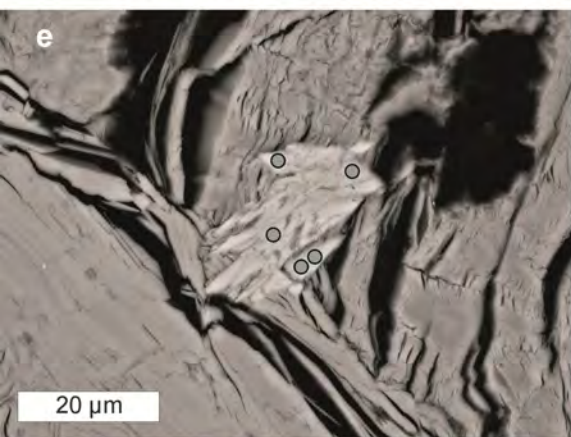
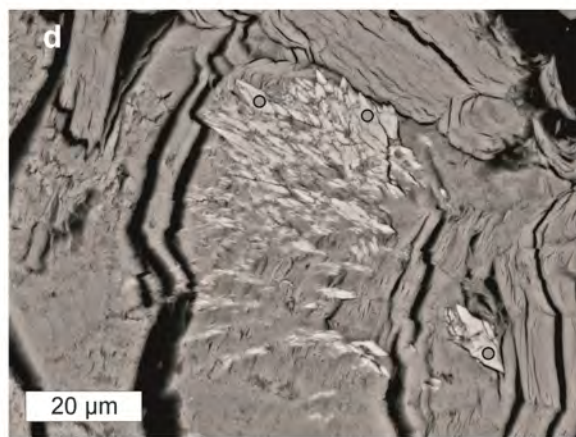
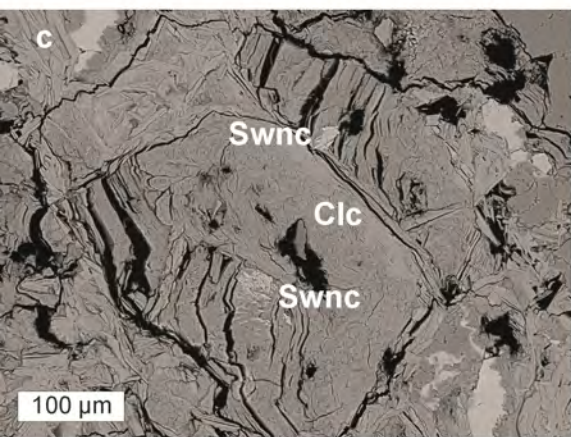
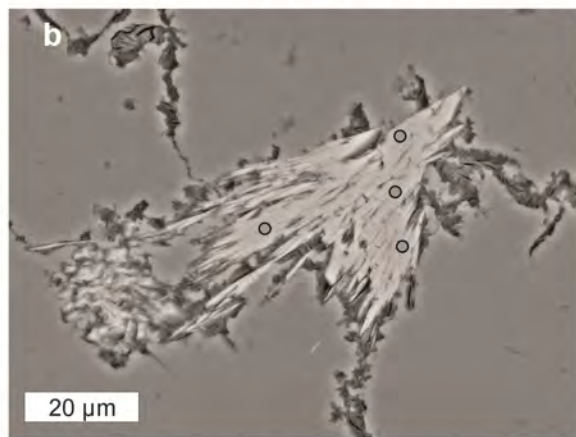
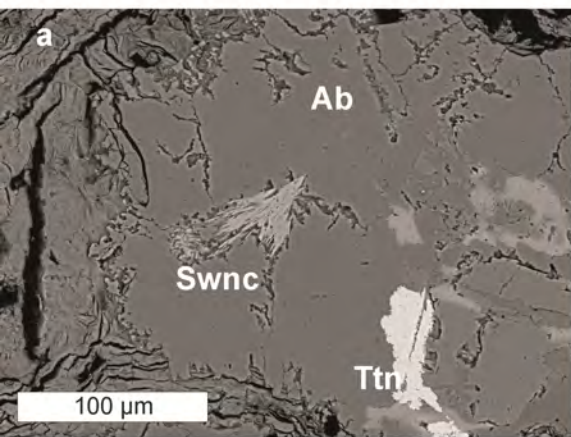


Fig. 3. Pieczka et al. Scandio-winchite

